Analytical and Bioanalytical Chemistry (2022) 414:4021–4037
https://doi.org/10.1007/s00216-022-04061-z

PAPER IN FOREFRONT

Label-free DNAzyme for highly sensitive detection of multiple biomolecules in real samples through target-triggered catalytic cleavage reactions with auramine O's discriminated fluorescence emission

Arunjegan Amalraj[1] · **Panneerselvam Perumal**[1]

Received: 17 February 2022 / Revised: 24 March 2022 / Accepted: 4 April 2022 / Published online: 23 April 2022

Abstract
A universal enzyme strand (E-DNA) recyclable L-histidine (L-His), melamine (MA), and cisplatin (CP) biosensor was fabricated on the basis of a target-specific RNA-cleaving DNAzyme with specific auramine O (AuO) dye instead of thioflavin T. In this strategy, the substrate strand (S-DNA) of the RNA-cleaving site was constructed as an intramolecular stem-loop structure, and a GT-rich sequence was imprisoned in the double-stranded stem which inhibits the formation of stable G-quadruplex (G4cpx) with AuO. The presence of L-His initiates a catalytic reaction for cleaving the RNA site of the S-DNA hydrolytically releasing the GT-rich portion, which subsequently combines with AuO and forms a G4cpx for enhanced fluorescent signal. The subsequent addition of MA uncoils the G4cpx to form T-MA-T dsDNA, or addition of CP unwound the G4cpx to form CP-DNA leading to an intensive decrease of AuO emission. Remarkably, the liberated L-His can ultimately cause several rounds of cleavage, and the liberated E-DNA can catalyze the subsequent reaction with the other S-DNA. The use of L-His and E-DNA repeatedly induces S-DNA cleavage and intensifies the emission signal. The results show that the proposed biosensor is extremely sensitive to L-His, MA, and CP with a detection limit of 0.98, 10, and 3.4 nM respectively. To the best of our knowledge, the utilization of AuO as the G4cpx inducer and stabilizer for L-His, MA, and CP detection in real milk and urine samples has never been reported.

Keywords L-His-trigger · RNA-cleave · Auramine O · T-MA-T · G-CP-G adduct

Introduction

L-Histidine (L-His) is a proteinogenic amino acid that plays a significant role in biochemistry due to its aromatic imidazole functional group. It can take an active part in a wide range of biological processes including cell activities, metabolic activity, and regulation, which are important for the growth and development of living activity. L-His is involved in the maintenance of healthy tissues as well as the protection of nerve cells that carry messages from the brain to various parts of the body. This also plays a role in hemoglobin function and structure, and one-carbon metabolism, all of which regulate gene expression and protein biological activity. Meanwhile, the oscillation of L-His content is an essential index to reflect a variety of potential diseases. However, it should be noted that excessive L-His may lead to some dangerous diseases such as arthritis, liver failure, kidney disease, AIDS, and cancer. On a contrasting note, recent studies have shown that a deficiency of L-His in plasma may lead to an impaired nutritional state in patients with chronic kidney disease, nerve deafness, and hepatic and renal degeneration [1, 2]. Therefore, the lack or excess amount of L-His is responsible for many diseases in people. Hence, the biological system must have an optimal level of L-His concentration.

Melamine (MA) is a low-toxic industrial raw ingredient that is used to make MA-formaldehyde resin, plastics, glues, and fertilizers. On the other hand, it is illegally added to milk products in order to increase the apparent crude protein (nitrogen content) at reduced cost, causing kidney disease and even death in humans (especially infants). Since MA

✉ Panneerselvam Perumal
panneerp1@srmist.edu.in; panneerchem82@gmail.com

[1] Department of Chemistry, SRM Institute of Science and Technology, Kattankulathur 603203, Tamil Nadu, India

cannot be metabolized in the human body, they can form insoluble complexes with cyanuric acid depending on urine pH, which can lead to crystallization and subsequent tissue destruction. In this way, an excessive intake of MA will result in the production of insoluble MA anurate crystals in the kidney and eventually induce renal failure. According to FDA standards for MA interim safety and risk evaluation, a maximum quantity of 20 μM MA can be present in food for human consumption [3–5].

Cisplatin (CP), an alkylating agent, is a highly effective chemotherapy drug that is widely used to treat a variety of cancers, which include testicular, cervical, head and neck, bladder, and lung cancer. Despite being a powerful anticancer medicine, its clinical scope is restricted due to its severe side effects on organs such as the kidney, liver, brain, and gastrointestinal tract. When CP is delivered to cells, the Cl^- ions separate from the positively charged platinum ions and interact with cellular DNA and proteins, inhibiting replication, transcription, translation, and DNA repair. However, CP administration has frequently resulted in toxic side effects such as nephrotoxicity, neurotoxicity, and nausea. Furthermore, CP at low concentration causes cell apoptosis, whereas CP at high concentration causes necrotic cell death [6, 7].

Traditional analytical methods such as high-pressure liquid chromatography, mass spectroscopy, atomic absorption spectroscopy, colorimetry, etc. are employed to detect the L-His, MA, and CP. However, these methods are costly due to their bulky setup, longer working procedure, complicated pre-treatment, large amount of sample, and low sensitivity. But, the electrochemistry voltammetry technique has been successfully used to measure the L-His, MA, and CP at low concentration. Nevertheless, this method also has some limitations such as proper maintenance of the working electrode, unstable current background, drifting of reduction and oxidation potential peak positions due to aging of the reference electrode, and the presence of a high concentration of common analyte ion in real samples [8–19]. Therefore, the development of rapid, highly sensitive, more accurate, and simple analytical methods for detecting L-His, MA, and CP especially for real-time and on-site scenarios becomes vital.

Over the last few years, in vitro nucleic acids have played a major role in the field of selective molecular recognition. A class of unique DNA sequences (DNAzymes) having the ability to bind neutral molecules and strong cleavage activity with its RNA substrates were utilized as a universal platform for neutral molecule sensing application. DNAzymes received substantial attention due to their amazing stability, specificity, and low cost when compared to ribozymes. Nowadays several DNAzymes have been discovered and used to create sensitive sensing platforms for a variety of targets. Among these DNAzymes, we have discovered a new single DNAzyme to detect multiple analytes. As a consequence, the researcher has transformed DNAzymes into extremely sensitive and selective neutral molecule biosensors using diverse signal transduction techniques such as fluorescence, colorimetric, and electrochemistry. Among them, the fluorescence-based DNAzyme biosensor has received prodigious attention for quantitative analysis of neutral molecules because it is the most competitive, simpler, and compatible [20].

To take advantage of DNAzymes' multiple enzymatic turnover property, the molecular beacon structure is used in the design of substrate for DNAzyme-based fluorescent sensing systems. However, all these sensors need covalent labeling of the DNAzyme with fluorophore and quencher parts in order to produce a well-organized signal output triggered by a target. This may necessitate a complex synthetic route design and several heavy and complicated synthetic stages, resulting in higher costs, higher time consumption, and lower synthesis yield. Furthermore, numerous fluorescent and quenching compounds may affect the recognition event, thereby interfering with the sensitive and selective detection of the targeted analyte. In response to these limitations, herein, we reported the label-free fluorophore and quencher DNAzyme-based fluorescence biosensor for detection of L-His, MA, and CP. In the label-free techniques, the fluorophores are not covalently bonded to the nucleic acid backbone. Instead, the fluorophore interacts with the DNA non-covalently via a variety of binding mechanisms, including intercalation, end-stacking, or electrostatic interactions. More interestingly, this reported approach does not need any external fluorescence quencher like nanomaterials (metal oxide, graphene oxide, MOF, etc.).

The luminous compounds used in the label-free DNA probes are usually non-emissive or slightly emissive in aqueous solution resulting in excited state quenching by solvent interactions. However, when bound to specified DNA structures, they exhibit increased luminescence due to the preservation of their excited states within the hydrophobic core of the DNA. Thus, the great benefit of the label-free DNA-based technique is that the detection may be done in a homogeneous solution without any pre-labeling or immobilization steps, significantly lowering the time and cost required for the experiment. Moreover, the inherent adaptability of label-free sensing makes it an ideal platform to be integrated with biomolecular technology with novel functionality, as in the case of the molecular tools provided by DNA nanotechnology [21, 22].

In the last few years, the researcher has reported the application of thioflavin-T (ThT) as a highly selective luminescent probe for the label-free detection of metal ions and biomolecules [23]. But now, there is an indispensable need for a highly efficient substitute fluorescence probe for ThT in the detection of targets. Here, we present the use of AuO as a potential alternative to ThT. The same as with ThT, the increase in AuO emission upon binding to DNA is due to the suppression of free rotation of the two dimethylamino arms

of the molecule. This inhibition prevents the excited-state electronic wave function from moving the emissive locally excited state to the dark charge-transfer state. In the earlier study, the photophysical properties of AuO have received increasing attention than those of ThT, and moreover, the spectroscopic sensitivity of AuO is even superior to that of ThT [24]. Therefore, we have described the application of AuO as a highly specific fluorescence indicator for the label-free DNAzyme-based biosensor for detection of biomolecules like L-His, MA, and CP.

Here, we have developed a simple and label-free DNAzyme/AuO-based sensor for the fluorometric detection of L-His, MA, and CP by recycled E-DNA for signal amplification. The S-DNA consists of a typical stem-loop structure. The loop of S-DNA, which has a similar sequence with E-DNA, could hybridize to form an intact DNAzyme structure. The L-His triggers cleavage of S-DNA resulting in the release of a GT-rich sequence and subsequent formation of a G4cpx with AuO, resulting in significant enhancement of the AuO emission. At the same time, the liberated L-His and E-DNA mediate a new cycle of cleavage and association of new DNAzyme respectively, resulting in the ultra-trace detection of L-His. Following this, the MA/CP was added, which interacts with the T/G base pairs in the G4cpx, uncoiling the G4cpx, and forms the T-MA-T dsDNA / CP-DNA adduct, leading to a decrease in AuO emission. The AuO and the proposed sensing mechanism have excellently supported multiple detections of organic pollutants in the milk and urine samples.

Materials and methods

Chemical and reagents

All of the E-DNA and S-DNA used in this study were developed by Allied Scientific Products (Kolkata, India) and purified using the HPLC technique. The supplementary tables S1 and S2 provide detailed information on all DNA sequences. The stock solution of DNA was made by dissolving 50 mM of Tris–HCl buffer and was kept at 4 °C. L-Histidine, melamine, auramine O, cisplatin, dopamine, urea, and tris hydrochloride buffer salt were obtained from Sigma-Aldrich and SRL Chemicals, India. All other chemicals (including various amino acids, metal salts, and drugs) were of analytical-reagent grade and used without further purification.

Structural characterization

The sensor's AuO excitation and emission intensities were measured using a spectrofluorometer (HORIBA JOBIN YVON Fluoromax-4), with light from a standard Xe lamp used as an excitation source. The UV–visible spectroscopy was used to measure absorption (Shimadzu, UV-2600). To optimize the pH of the sensing system, a digital pH meter (PHS-3C) was used. The CD spectroscopy was used to confirm the DNA structural changes.

Detection procedure

The analytical technique for multiple detection of L-His, MA, and CP biosensor was explored as follows: At first, the DNAzyme hybridization reaction was implemented by mixing the pre-heated and cooled S-DNA (2 µL) and E-DNA (1 µL) at room temperature for 10 min in the 50 mM Tris–HCl (pH 7.4). For catalytic cleavage reaction, 10 µL of L-His solution of an appropriate concentration was added to the above solution. Subsequently, the mixture was treated with AuO (10 µM) for 10 min at 37 °C to form the AuO-G4cpx, indicating the significantly enhanced AuO fluorescence emission at excitation and emission wavelengths of 425 and 515 nm, respectively. Further, the AuO-G4cpx functioned as a sensitive probe for MA and CP detection. Therefore, an appropriate concentration of MA and CP was subsequently added into the above solution, which resulted in a considerable emission of the AuO emission.

Real-sample analysis

We hoped that our DNAzyme/AuO–based probe would be capable of detecting L-His and MA in food samples such as milk. Milk samples were collected from local supermarkets in Tamil Nadu, India, near the SRMIST. To summarize, the milk was mixed with acetonitrile and trichloroacetic acid. The resulting mixture was centrifuged at 10,000 rpm/min for 10 min after 30 min of sonication to dissolve the organic materials. The obtained supernatant was filtered, diluted 25-fold with buffer, and then used to perform L-His and MA analysis under the optimal conditions. Surprisingly, the proposed sensing probe is also adept at subsequently detecting L-His and CP in urine samples. The urine samples were brought from a urine testing laboratory in Chennai, Tamil Nadu, India (their consent was recorded). Urine samples were filtered through a membrane to remove all insoluble impurities prior to quantitative analysis of L-His and CP. A stock solution of L-His and CP diluted with buffer was spiked into aliquots of the urine samples. The fluorescence records were then carried out.

Results and discussion

Analysis of E-DNA and S-DNA sequence

The E-DNA binds with the S-DNA in two duplex regions, and the middle portion is the catalytic core. Herein, we analyze the binding stability of E-DNA on S-DNA as it

forms a more stable complex which leads to a decrease in the S-DNA cleaving ability. This highly affects the proposed sensor performance in terms of sensitivity and detection accuracy. Thus, we have designed ten E-DNA with different binding sites of S-DNA to find out the most suitable E-DNA. The different designed substrate-binding arms are highlighted, and the remaining sequences exist as the catalytic core sites. Each E-DNA in table S1 was individually hybridized with the S-DNA. Further, the efficiency of the E-DNA was analyzed in the presence of L-His and AuO (Fig. 1a). As per the experimental results, the E-DNA 7 was found to have significant cleavage in 10 min which produced the effective AuO fluorescence emission process. The other few E-DNA exhibited reduced fluorescence emission, and some of the E-DNA exhibited no fluorescence emission. This is due to enhanced stable interaction between the E-DNA and S-DNA, resulting in the formation of highly stable DNAzyme (E-DNA and S-DNA hybridization). The schematic representation of E-DNA and S-DNA is shown in Fig. 1b. Furthermore, the stepwise analysis of S-DNA sequence is shown in table S2 which involves selection of the S-DNA stem length, quantity of G-quartets in portion 1 S-DNA, loop length of G4cpx and sensitivity analysis of MA and CP on S-DNA 4E (portion 1) were discussed in SI Sect. 1.0.

Sensitivity contrast between AuO and ThT dye

In the past decades, the researcher has reported the ThT as a cost-effective fluorescent probe in label-free sensor application but, in this proposed biosensor, the AuO is used as a great substitute for ThT. Therefore, we have examined the sensitivity of both ThT and AuO for the detection of targets as no one reported the AuO utilized biosensor for the detection of L-His, MA, and CP. The results of fluorescence studies revealed that changes in fluorescence of the AuO and ThT in the presence of targets are nearly identical, as shown in Fig. 2a, b. In addition, the sensitivity percentage histogram clearly illustrates that the AuO possesses little higher sensitivity (Fig. 2c) due to the superior spectroscopic sensitivity of AuO than ThT. Thus, we have used AuO as the best fluorescent indicator for the detection of L-His, MA, and CP.

The proposed sensing mechanism

The label-free fluorescent strategy for L-His, MA, and CP sensing based on the selective DNAzyme and AuO is shown schematically in Scheme 1. The AuO is a novel probe for L-His, MA, and CP detection due to its ability to increase fluorescence brightness by forming G4cpx, but not with dsDNA and ssDNA. The selective DNAzyme was composed of an enzyme (E-DNA) and a substrate strand (S-DNA). The S-DNA sequence is composed of two parts: the specific GT-rich region (color portion 1) at the 5′ end was complementary to (color) portion 2 at the 3′ end, and in the middle of the substrate strand, a ribo-adenine (rA) was introduced as the cleavage site to L-His. The hybridization between them causes the S-DNA to form a molecular beacon stem-loop structure, with the E-DNA-binding sites in the middle of the loop. The formation of a G4cpx is prevented by the G-rich

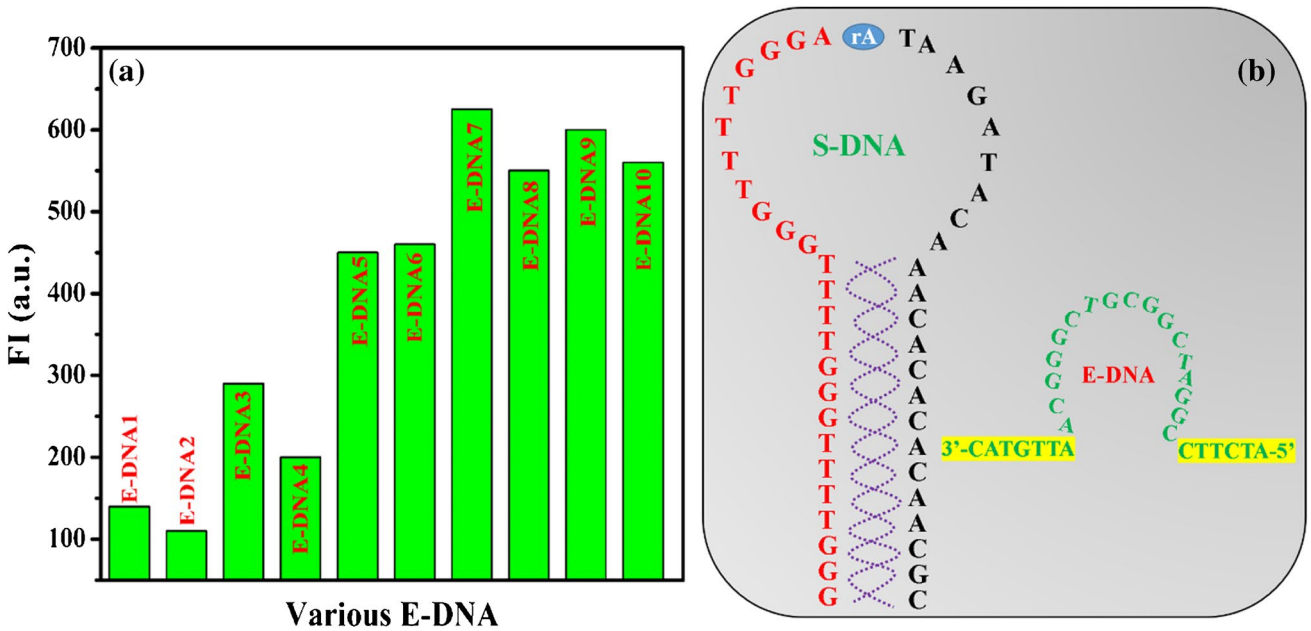

Fig. 1 **a** Comparison of various E-DNA sequences, **b** schematic diagram for S-DNA and E-DNA

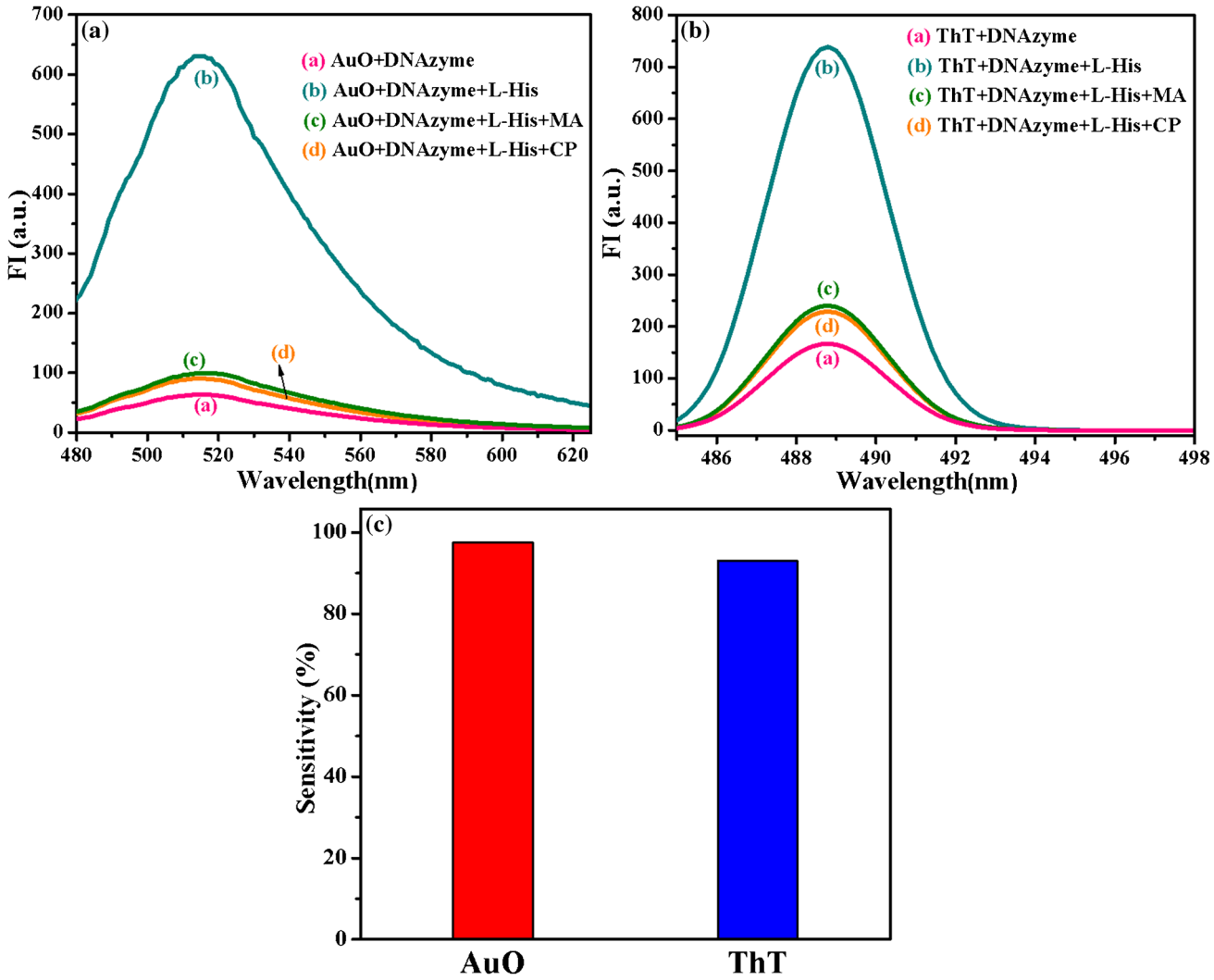

Fig. 2 Detection of targets by using **a** AuO and **b** ThT. **c** Percentage of detection sensitivity with AuO and ThT

sequence being partially caged in the double-stranded stem. The structure of DNAzyme was so stable in the absence of L-His that the primers of the cleavage reaction were blocked in it, and DNAzyme remained stable in their hairpin structure. As a result, after adding AuO, the fluorescence signal was weak. Whereas, in the presence of L-His, the catalytic trans-acting reactions were initiated for the hydrolytic cleavage of the S-DNA at the scissile (phosphodiester) rA into two fragments and dissociated from the E-DNA. The E-DNA would break free from the S-DNA and form a hybrid with the other S-DNA, which would trigger the next cleavage process. In this stage, the E-DNA is recycled to create the first amplified signal. The cleavage activity deformed the DNAzyme stability, liberating the L-His and portion I (GT-rich) and II. The free L-His initiated the next phase of S-DNA cleavage with DNAzyme. Each released L-His can ultimately cause several rounds of cleavage, releasing portion I and portion II. Further, the liberated portion I (GT-rich sequence) coiled together into G4cpx in the presence of AuO dye (G4cpx-AuO) due to the π stacking interaction between the guanine bases and AuO and the protonated imine group between two electron-rich nitrogen atoms in its structure leads AuO to be a molecular fluorescent rotor. The interaction of AuO in G4cpx DNA prevents the rotation of the C–C bond in AuO structure and prevents the intramolecular charge transfer from an emissive to a nonradiative state [25], resulting in the remarkable AuO emission. The increase in fluorescence intensity was computed as the signal gain for the L-His quantification through F/F_0, where F_0 and F are the fluorescence intensities before and after the L-His DNAzyme reaction, respectively. Furthermore, the AuO-G4cpx system was used for the subsequent detection of MA or CP. Surprisingly, when MA was added into the G4-AuO system, owing to the affinity between the MA and thymine in

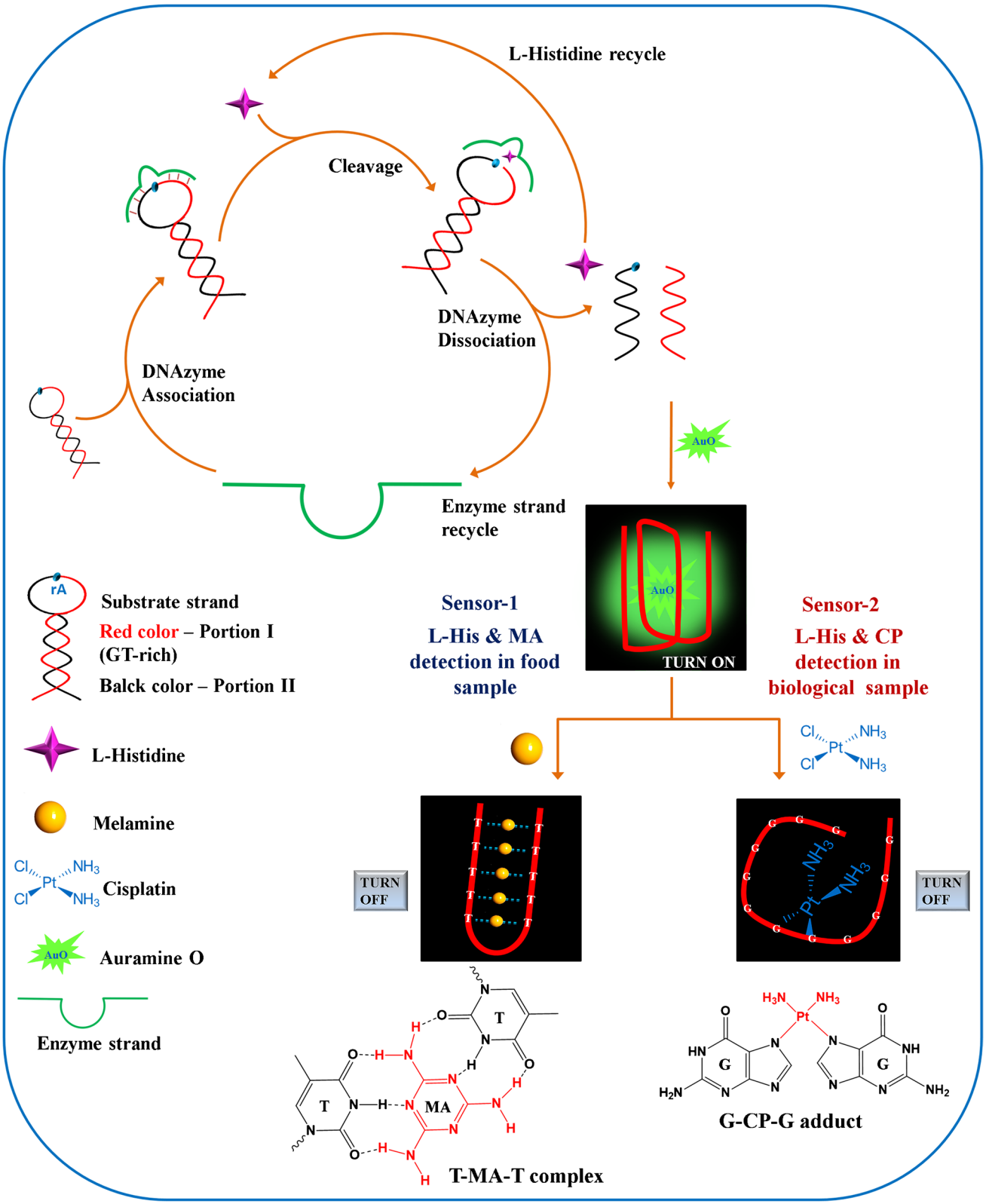

Scheme 1 Schematic representation for detection of L-His, MA, and CP

the G4cpx, the MA specifically reacts with thymine to form the "T-MA-T mismatch" structure, leading to a reduction of AuO fluorescence intensity. Unpredictably, the CP was added instead of MA, which also remarkably decreased the

AuO emission. This is due to the disappearance of AuO-G4cpx to the form stable CP-DNA adduct via G-CP-G interaction. Therefore, the formation of a G4cpx, T-MA-T duplex, and G-CP-G adduct structure was confirmed by the turn-ON and OFF fluorescence intensity of the AuO, UV–vis, and CD spectrum and the L-His triggered DNAzyme cleavage was confirmed by page gel experiment and cleavage reaction rate constant were shown in Figure S2a & b. Moreover, the target's detection can be visualized by color change of AuO under UV light.

Feasibility study

The AuO spectra of four distinctive samples were recorded initially to prove the strength of the suggested biosensor. As shown in Fig. 3a, initially, the AuO displays very weak emission (curve a) because of a highly efficient non-radiative structural relaxation mechanism that occurs in the excited state of AuO. In the excited state, this structural relaxation is recognized as a phenyl group twisting motion. Further, the AuO was incubated with DNAzyme, resulting in the weak fluorescence emission (curve b). However, in the existence of L-His, it initiates catalytic reactions to hydrolytically cleave the RNA site of the S-DNA and release the GT-rich part, which folded up into the G4cpx with the help of the AuO dye (AuO-G4cpx). Also, the fluorescence emission of AuO enhanced to a most remarkable degree (curve c) due to the impedance in a confined environment for the phenyl group twisting motion. The subsequent detection of MA was also done using an AuO-G4cpx system. The MA was inducted into the AuO-G4cpx system to unfold the G4cpx into a rigid DNA duplex structure due to the formation of three hydrogen bonds between the thymine base pair and the MA (T-MA-T). This releases free AO, thus transducing the DNA MA hybridization into a signal and the AuO emission yield of AuO decreased (curve d). The subsequent detection of CP was done using an AuO-G4cpx system. To the AuO-G4cpx system, the CP was induced to unfold the G4cpx into the CP-DNA adduct (G-CP-G). This also resulted in a dramatic decrease in the AuO emission (curve e). Thereby, we conclude that AuO serves as a ''light-up'' fluorescent folder and the stabilizer of the G4cpx.

Furthermore, the UV–vis absorption spectra of AuO were also investigated to confirm the formation of G4cpx, T-MA-T, and CP-DNA structure as shown in Fig. 3b. The characteristic absorption peak of AuO was 435 nm (curve a). When G4cpx was formed, the red shift from 432 to 444 nm was observed (curve b). In the presence of MA, the peak was similar to AuO because the G4cpx was uncoiled by forming DNA double strands (T-MA-T) (curve c). When CP was added instead of MA, the absorption peak was also identical to that of AuO. This was because the G4cpx unfolded to form a CP-DNA adduct (curve d). All the above results confirmed the feasibility of the proposed method to detect L-His, MA, and CP.

More interestingly, the detection of L-His, MA, and CP could be appropriately seen by the bare eye under the UV illumination at 365 nm, which provided a superficial technique for the visual recognition of targets. The original non-emissive AuO solution emitted a vivid green fluorescence under 365 nm ultraviolet rays, which confirmed that the AuO

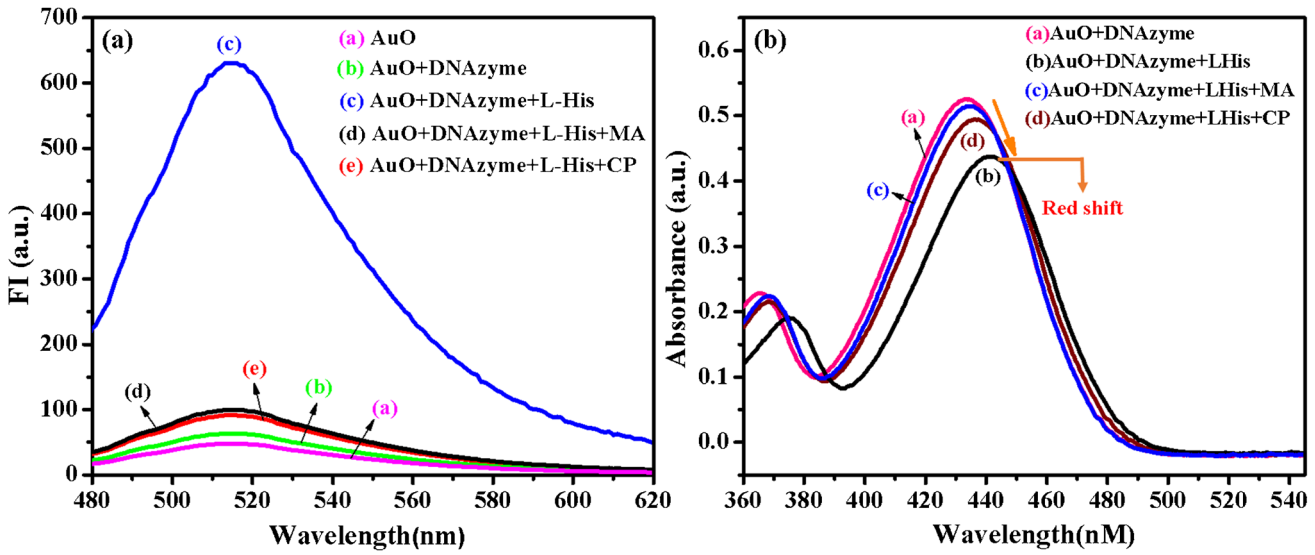

Fig. 3 **a** The changes in fluorescence emission under different conditions. (a) AuO alone; (b) AuO with DNAzyme; (c) AuO and DNAzyme with L-His; (d) AuO, DNAzyme, and L-His with MA; and (e) AuO, DNAzyme, and L-His with CP. **b** UV absorption of AuO. (a) AuO with DNAzyme; (b) AuO and DNAzyme with L-His; (c) AuO, DNAzyme, and L-His with MA; and (d) AuO, DNAzyme, and L-His with CP

facilitated a G4cpx production in the absence of a monovalent cation. When MA was added, the vivid green color faded to colorless, indicating the disappearance of the AuO-G4cpx complex and the formation of the duplex DNA. When CP was added instead of MA, the vivid green color became colorless, indicating the disappearance of the AuO-G4cpx complex by the formation of CP-DNA adduct (Figure S2).

Sensing confirmation by optical spectroscopy

Confirmation of the DNAzyme cleavage by L-His

The duplex-like substrate DNA cleaved into the ssDNA by the addition of L-His, which was experimentally confirmed and the schematic representation for RNA cleavage reaction as shown in Fig. 4A. Figure 4B (inset left) shows the UV bands of DNAzyme in the existence and non-existence of L-His. The absorption density increased as L-His was introduced, indicating cleavage of the S-DNA into ssDNA. The phenomenon of increased UV absorbance by the ssDNA is known as the hyperchromic shift. The purine and pyrimidine bases in ssDNA strongly absorbed the UV light, but the dsDNA adsorbed less strongly due to the stacking interaction between the bases. Furthermore, the AuO with DNAzyme exhibits a strong peak at 432 nm; however, in the presence of L-His, the spectra gradually decrease the intensity and the maximum shifts toward the red, moving from 432 to 444 nm for bound AuO (inset right). Hypochromic and bathochromic effects are often anticipated as an indication for AuO dye intercalation [25].We employed circular dichroism spectroscopy (CDS) to further prove the conformational change in the DNAzyme caused by L-His. Figure 4C shows a strong positive peak at 274 nm, and a negative peak at 243 nm, and these peaks correspond to the characteristics peak of the duplex DNAzyme (curve a). However, in the presence of L-His, the CD shows a less intense positive peak at 274 nm and a negative peak at 243 nm, and these peaks correspond to the characteristic peak of ssDNA [26] (curve b), which evidently proves the dissociation of DNAzyme into ssDNA (portions I and II). Moreover, the addition of L-His along with AuO into the DNAzyme resulted in the formation of an antiparallel G4cpx structure, which displayed a positive band at 245 nm and 295 nm and a negative band at 265 nm [27] (curve c). This also confirms the DNAzyme dissociation

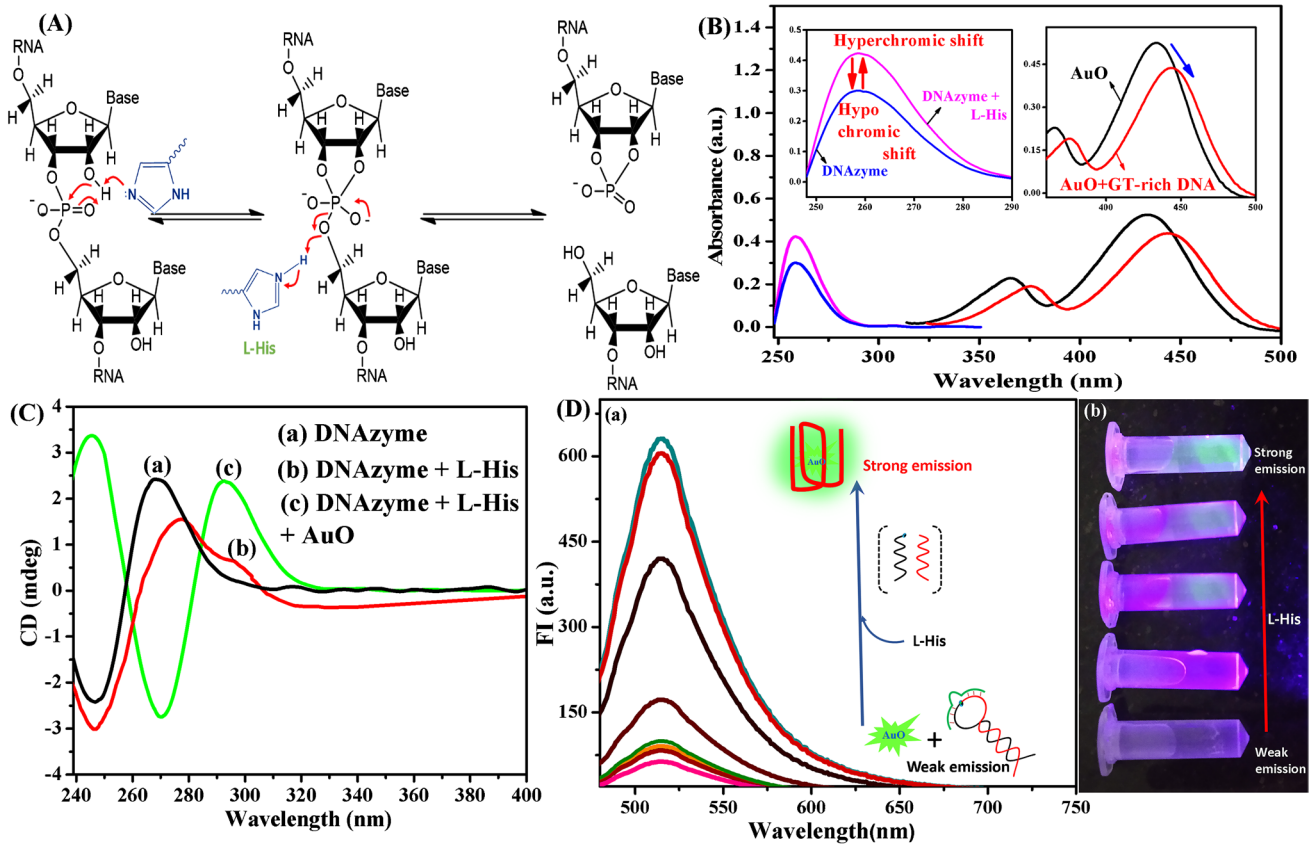

Fig. 4 **A** RNA cleavage reaction by L-His. **B** Study of UV spectroscopy; **C** CD spectroscopy; **D** study of (a) fluorescence spectroscopy and (b) UV light illumination for confirmation of RNA cleavage by L-His

into ssDNA by the L-His. Furthermore, the consequence of various amounts of L-His on the emission of the AuO could also be identified accurately by the fluorescence spectra and the naked eye, as demonstrated in Fig. 4D (a and b) respectively. The AuO fluorescence emission was gradually enhanced due to the formation of DNA G4cpx by the dissociation of DNAzyme into two portions.

Confirmation of melamine-induced DNA duplex structure

Next, we further investigated the binding of the GT-rich ssDNA with MA (Fig. 5A) through a combination of UV–vis and CD spectra. In the presence of MA, it was experimentally confirmed that the ssDNA formed dsDNA with the assistance of hydrogen bonding between thymine and MA. Figure 5B shows the UV absorption spectra of GT-rich ssDNA (267 nm) before and after the addition of melamine. The UV absorption density decreased upon the addition of MA, indicating the transition into a secondary structure of DNA. The phenomenon of decreased UV absorbance by the dsDNA compared to the ssDNA is known as a hypochromic effect. CDS revealed significant structuring of the GT-rich ssDNA in the presence of MA into AuO-G4cpx, all the characteristic peaks of the AuO-induced G4cpx disappeared, which resulted in the formation of a new positive peak at 280 nm corresponding to the characteristic peak of (T-MN-T) dsDNA [28] (Fig. 5C). Therefore, the results reproduced the features of the melamine-induced duplex formation in an excellent manner. Furthermore, the outcome of various amounts of MA on the emission of the AuO-G4cpx could also be accurately confirmed by the fluorescence spectra and the naked eye, as demonstrated in Fig. 5D (a and b). The AuO fluorescence emission was gradually quenched due to the formation of a DNA duplex structure by the dissociation of AuO-G4cpx, as seen in the spectra and photographs.

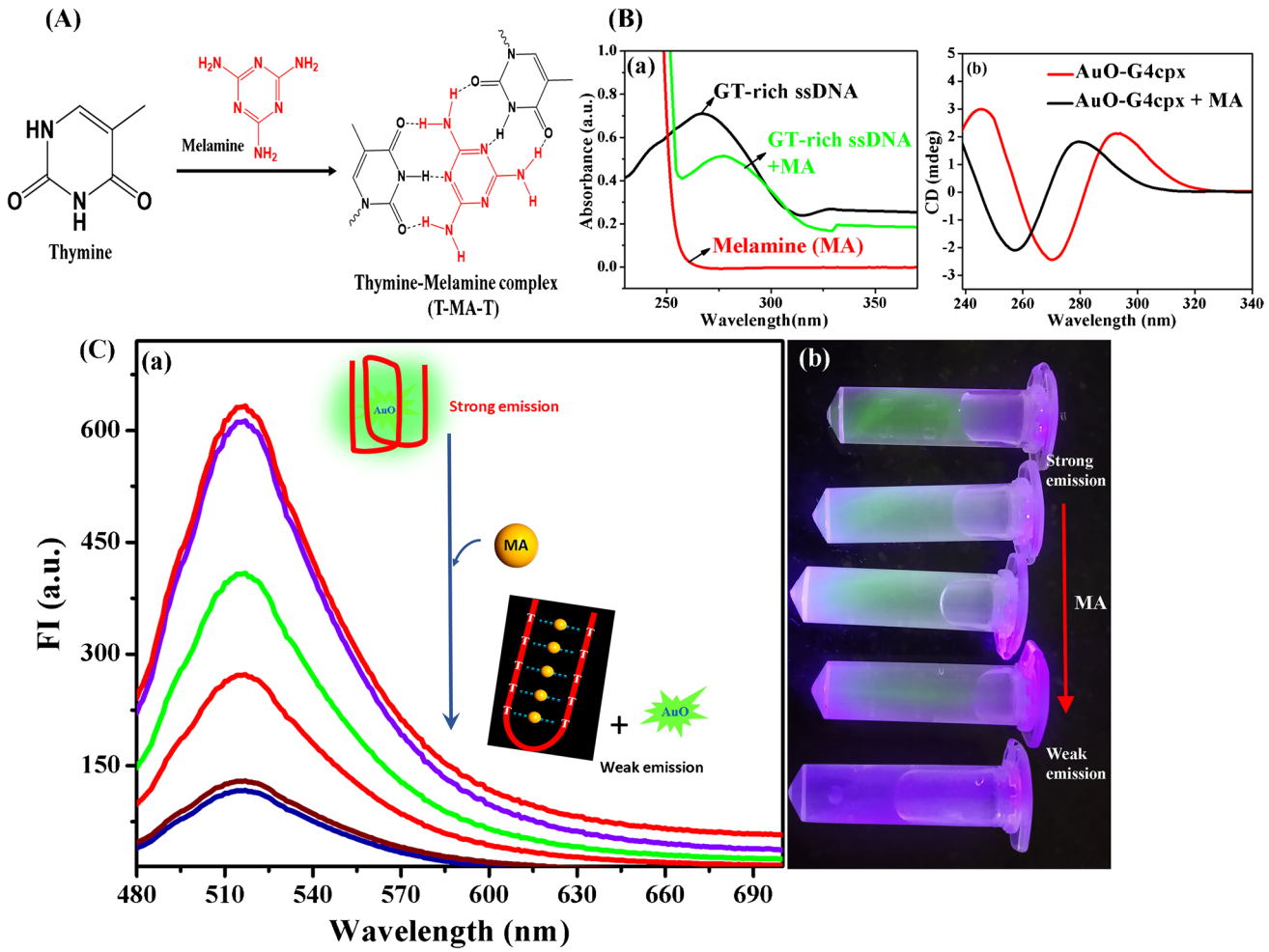

Fig. 5 **A** Reaction for the formation of T-MA-T complex. **B** Study of (a) UV spectroscopy and (b) CD spectroscopy for confirmation of DNA-melamine complex formation. **C** Study of (a) fluorescence spectroscopy and (b) UV light illumination for confirmation of DNA-melamine complex formation

Confirmation of cisplatin–DNA adduct from G4cpx

UV/Vis and CD spectroscopy were used to monitor the CP reaction with DNA (Fig. 6A). The typical UV band for DNA, which is centered at 260 nm, experiences a significant bathochromic shift from 260 to 269 nm, as seen in Fig. 6B, confirming the creation of numerous Pt-nucleobases covalent adducts. As illustrated in Fig. 6C, the CD studies revealed significant changes in the distinctive AuO-G4cpx spectra during the addition of CP. All the AuO-induced G4cpx CD peaks vanished to form a new positive peak at 280 nm, which was attributed to the formation of Pt-nucleobases covalent [29, 30]. Moreover, as validated in Fig. 6D (a and b), the result of various amounts of CP on the emission of the AuO/G4cpx could also be suitably sensed by the fluorescence spectra and naked eye, which provided a superficial technique for the accurate and visual detection of CP. The spectra and photographs showed that the AuO emission was steadily quenched due to the formation of CP-DNA adduct from the AuO-G4cpx.

Sensitivity performance of L-His, MA, and CP detection

The sensitivity and dynamic range of the biosensor were investigated for multiple detections of L-His, MA, and CP before being well optimized, and the optimization results were shown in SI Sect. 2.0. A series of L-His solutions were prepared with different concentrations and then analyzed using our L-His sensor. Figure 7a shows the fluorescence spectra of the AuO-G4cpx in the presence of L-His from 0 to 3000 nM. The fluorescence intensity increased noticeably as the quantity of L-His increased, indicating effective cleavage of the S-DNA to liberate a more GT-rich portion for folding the G4cpx by AuO. Figure 7b depicts the calibration curve of the L-His biosensor, which achieved a dynamic range of 0 to 3000 nM with a linear relationship range up to 15 nM (Fig. 7b (inset)). A detection limit of 0.98 nM for L-His was expected according to the 3σ method ($R^2 = 0.9942$), which was much lower than almost all of the earlier-described sensors for L-His. As shown in Table S3, the results indicate that the

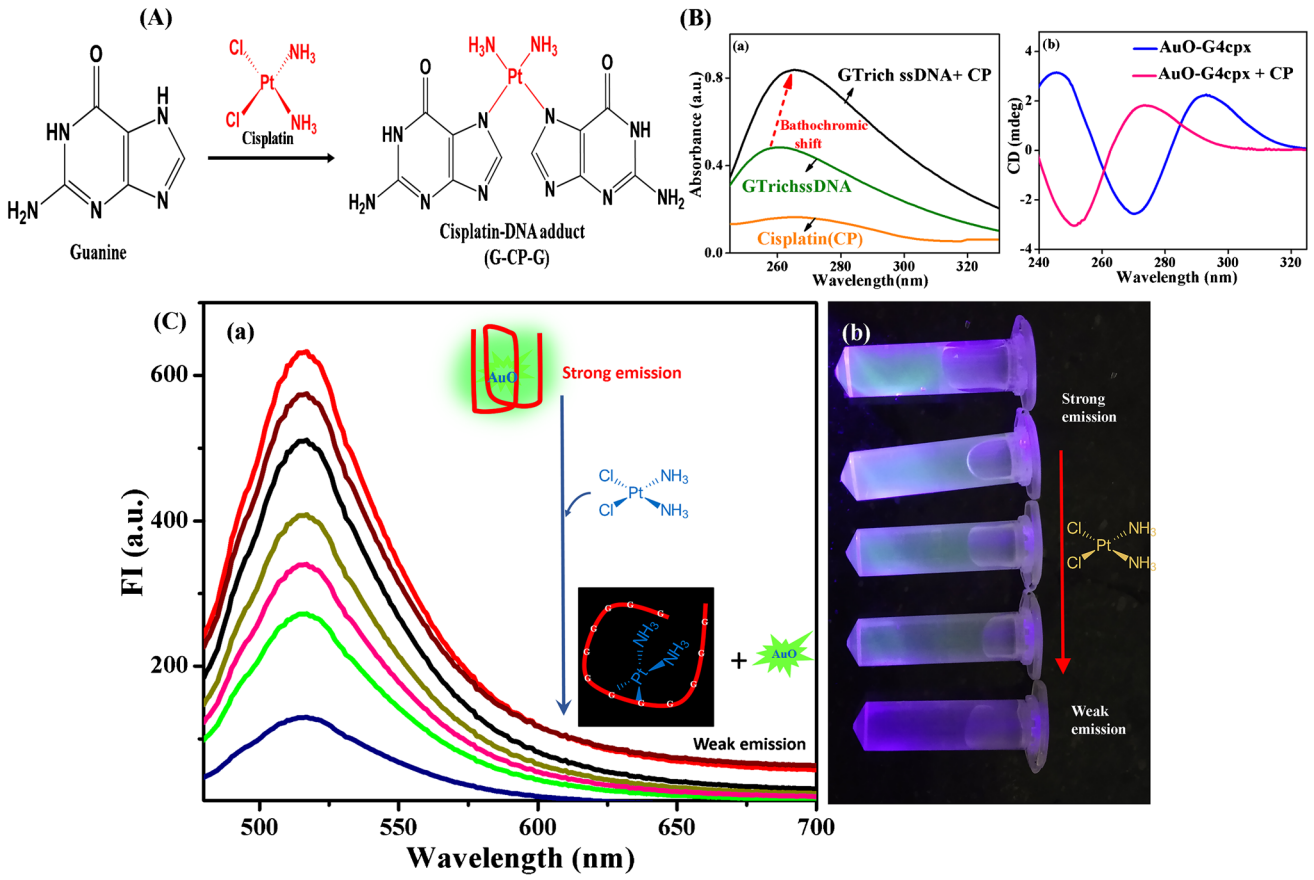

Fig. 6 **A** Reaction between DNA and CP. **B** Study of (a) UV spectroscopy and (b) CD spectroscopy. **C** (a) Fluorescence spectroscopy and (b) UV light illumination for confirmation of DNA-cisplatin adduct formation

proposed L-His sensor is sufficient for the detection of L-His in the milk and urine samples.

Next, the following addition of MA has efficiently turned off the fluorescence emission of the AuO-G4cpx system, which serves as an efficient detection probe for MA. Therefore, a series of concentrations of MA from 0 to 25 µM were separately added to the AuO-G4cpx system. Figure 8a reveals the fluorescence spectra of AuO-G4cpx to different concentrations of MA. As the concentration of MA increases, the AuO signal significantly decreases,

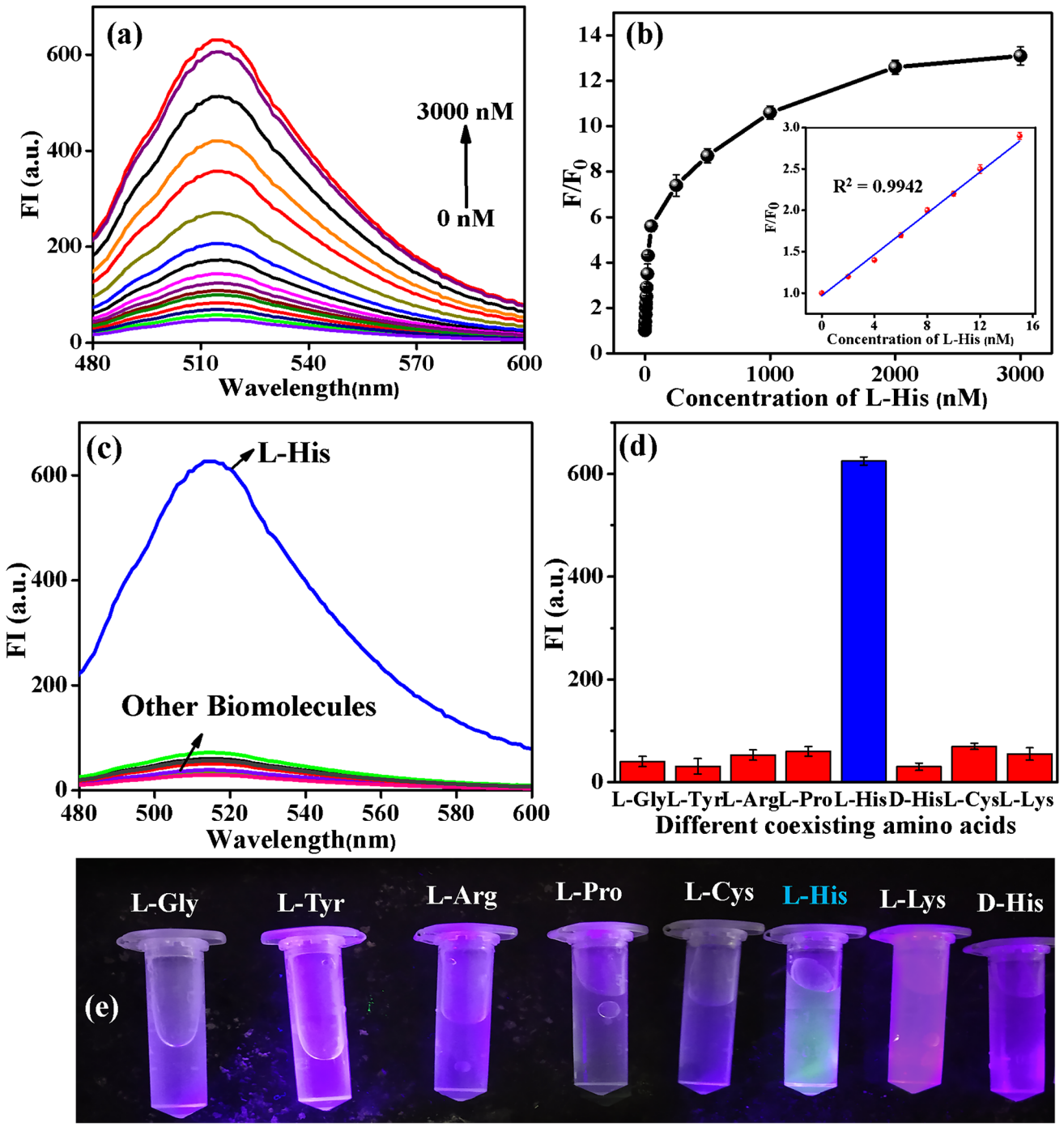

Fig. 7 Fluorescence-enhanced **a** spectra for AuO at different concentrations of L-His (0, 2, 4, 6, 8, 10, 12, 15, 20, 25, 50, 250, 500, 1000, 2000, 3000 nM). **b** Relationship of emission versus the L-His concentrations. **b** (inset) Linear relationship between fluorescence intensity and L-His concentrations (0–15 nM). Selectivity study for L-His with other coexisting biomolecules **c** fluorescence spectra, **d** histogram representation, and **e** visual detection of L-His

indicating the conversion of AuO-G4cpx into MA-duplex structure through T-MA-T. Figure 8b shows the calibration curve for the concentrations of MA versus fluorescence intensity. The Fig. 8b inset displays a good linear relationship (correlation coefficient $R^2 = 0.9911$) between the relative fluorescence emission and concentration of MA in the range from 0 to 1.5 μM. The limit of detection was calculated to be 10 nM defined by the equation LOD = 3σ/slope. The comparison of our detection probe with other previously reported sensors in terms of detection sensitivity and feasibility is outlined in Table S3. In comparison to other previously reported MA detection sensors, our detection approach has superior sensitivity and selectivity.

On the other hand, the subsequent addition of CP instead of MA also efficiently turned off the AuO emission of the AuO-G4cpx, which provided an effective CP sensing probe. To examination the recognition range of this recognizing approach, different concentrations of CP (0–1000 nM) were added to the experimental system. With cisplatin concentrations up to 1000 nM, the fluorescence intensity decreased (Fig. 9a).These results demonstrated that the structural distortion of AuO-G4cpx was directly associated to the concentration of CP. The fluorescence emission change ratio (F/F_0) increased with different CP concentrations (Fig. 9b), and the Fig. 9b inset shows a good linear relationship from 0 to 30 nM of CP ($R^2 = 0.9954$). The LOD for CP was estimated to be 3.4 nM, which was better or comparable to the LOD obtained by other methods (Table S3).

Selectivity performance of L-His, MA, and CP detection

Selectivity of the L-His probe was also explored, and the fluorescence response of other (L-Cys, L-Tyr, L-Arg, L-pro, L-Lys, L-Gly, and D-His) amino acids was also investigated. They commonly coexist in real biological and food samples. The photoluminescence response of the proposed sensing probe to L-His (100 nM) was more prominent compared to the other amino acids (500 nM), as shown in Fig. 7c, d. These studies indicated that the sensor could discriminate L-His from other compounds. The selectivity of the sensor was further validated by comparing two mixed solutions containing all the amino acids with and without L-His. Despite the presence of the interfering amino acids, the detection probe shows excellent selectivity for L-His. It was confirmed that only the L-His was capable of triggering the RNA cleavage and releasing the substrate DNA, which was folded up into G4cpx by AuO. Moreover, the color variations of the assay solutions also confirm that these amino acids do not interfere with the assay. The sample solution containing L-His was green in color, which visually indicated the formation of AuO-G4cpx, whereas all other samples revealed an absence of color under UV irradiation (Fig. 7e).

Further, the AuO-G4cpx serves as a detection probe for MA and CP. Therefore, the selectivity of the MA sensor was evaluated by testing the AuO-G4cpx with other compounds, including ascorbic acid, vitamin B, lactose, sucrose, Ca^{2+}, Cu^{2+}, Fe^{3+}, Mg^{2+}, and glucose, each at a concentration of 1000 nM. The photoluminescence response of AuO-G4cpx is being used to analyze MA sensing. As revealed in Fig. 8c, d, the majority of common materials in dairy foods and analogs of melamine display relatively insignificant interferences at the 1000 nM level on the identification of 50 nM melamine. Obviously, such high selectivity results from the thymine's selective recognition of melamine, i.e., stable triple hydrogen bonding between MA and T bases. It should be noted that the Hg^{2+} mix can also be stabilized in the T-T (T-Hg-T) process, i.e., the Hg^{2+} is a possible MA detection interferent. Luckily, in milk-based samples, there is a substantially lower abundance of Hg^{2+} than melamine. This is because melamine can artificially be added to increase the nitrogen content. Also, Hg^{2+} does not come from such an artificial source.

In the detection of CP, the selectivity analysis was also conducted with other anti-cancer drugs. All the anti-cancer drugs tested, including CP, have a concentration of 500 nM, as shown in Fig. 9c, d. Only the CP test produced significantly lower fluorescence emission. In addition, the reaction mechanism of oxaliplatin and carboplatin was fairly related to that of CP, and the interfering between them was also studied (Fig. 9e). The AuO emission of the reaction of G4cpx along with abovementioned drugs at 500 nM was studied before and after adding an identical quantity of CP. Agreeing to the data, the AuO signal of carboplatin was practically vague from the blank. The AuO signal of oxaliplatin was equally strong. Both signals considerably exhibited greater fluorescence emission than CP. The reason is that oxaliplatin and carboplatin have weaker leaving groups than CP, which slows the formation of adducts and makes the displacement of AuO from G4cpx very difficult. However, all the signals increased in a very slow manner after the addition of CP, as the existence of oxaliplatin and carboplatin did not disturb the CP outcomes in the optimized conditions. This is due to the strong binding attraction between CP and G-bases with the assistance of the robust covalent bond. This explained the outstanding discrimination among all the verified drugs, whereas the selectivity between platinum complexes could be attributed to a significantly higher rate of Pt–DNA formation in CP compared to oxaliplatin and carboplatin. We too verified the biosensor response compared to main molecules (dopamine, Na^+, K^+, Cl^-, and urea) often found in normal urine at high concentrations. Figure 9f shows that, even in the existence of such potentially interfering

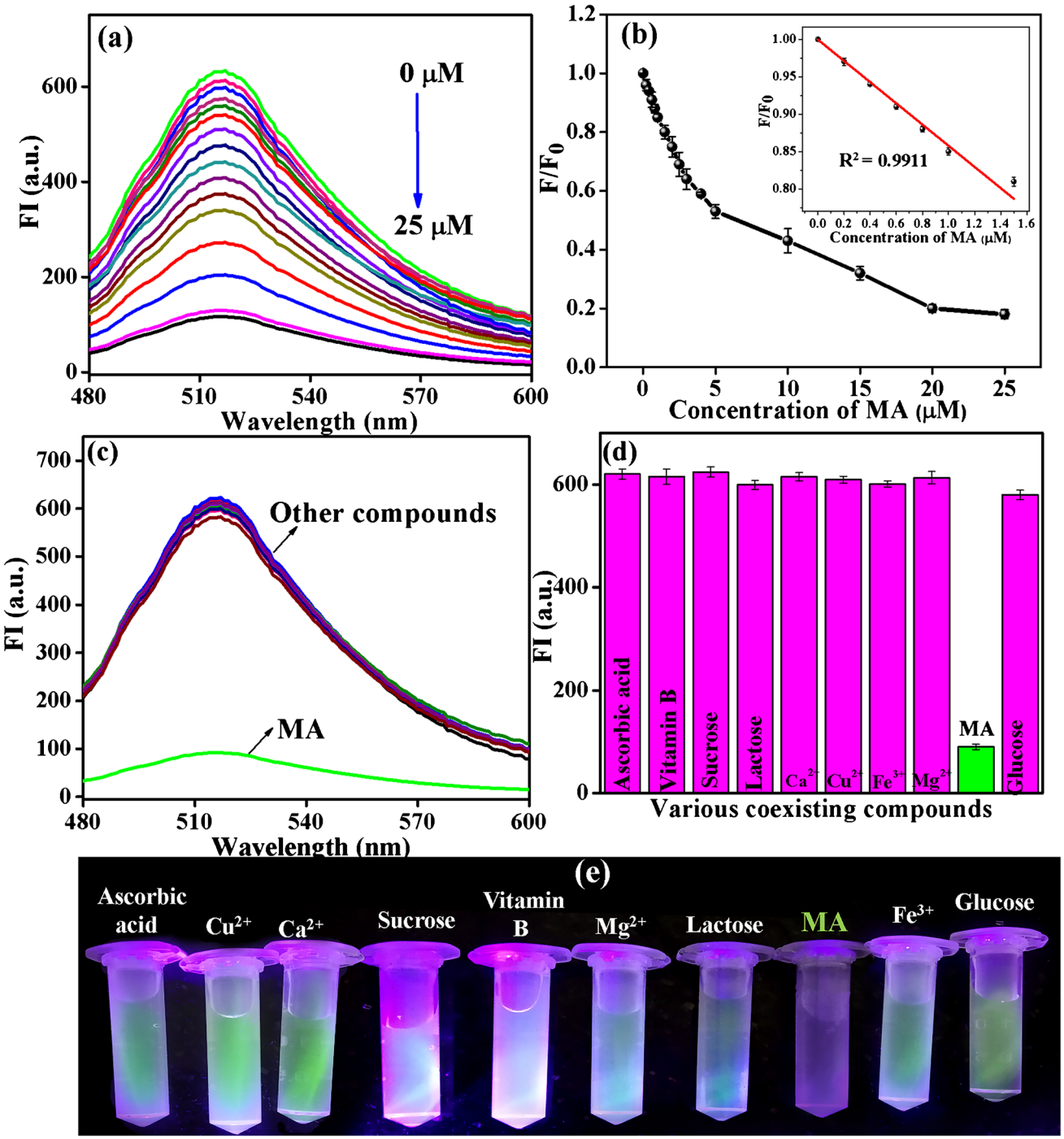

Fig. 8 **a** Fluorescence quenched spectra for AuO with dissimilar amounts of MA (0, 0.2, 0.4, 0.6, 0.8, 1, 1.5, 2, 2.5, 3, 4, 5, 10, 15, 20, and 25 μM). **b** Relationship of emission versus the MA concentrations; **b** (inset) linear relationship between fluorescence intensity and MA concentrations (0–1.5 μM). Selectivity study for MA with coexisting other compounds' **c** fluorescence spectra and **d** histogram representation and **e** visual detection of MA

molecules, the sensor response remained constant. Hence, this proves the sensor's good selectivity toward CP. Moreover, under UV irradiation, the color changes of the MA and CP assay solutions also visually confirm that these different compounds did not interfere with the assay. The sample solution containing other compounds revealed green color, whereas the sample containing MA or CP turned greenish color into a colorless form which visually indicated the formation of the MA-duplex or CP-DNA adduct as shown in Figs. 8e and 9g.

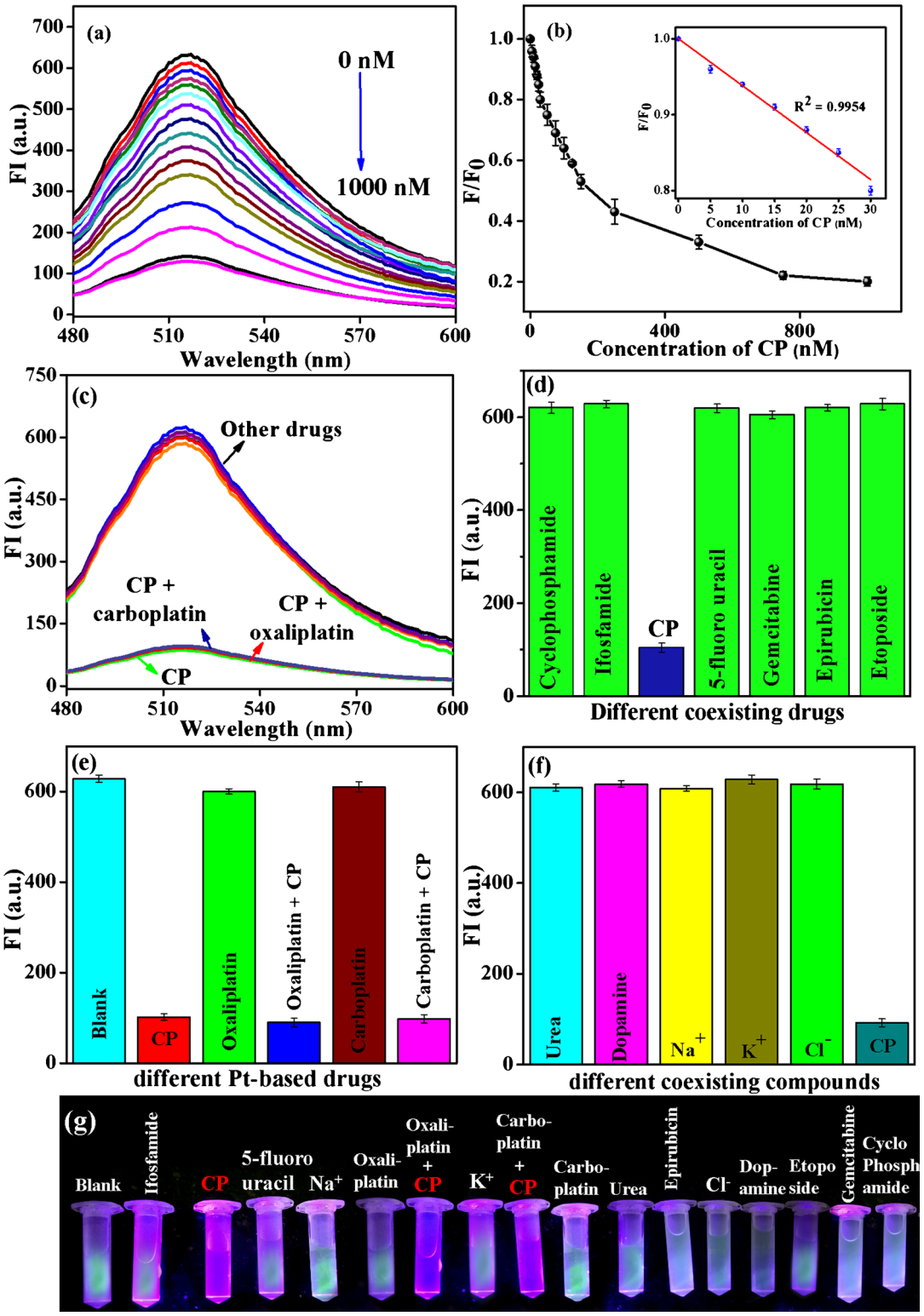

Fig. 9 **a** Fluorescence quenched spectra for AuO at different concentrations of CP (0, 5, 10, 15, 20, 25, 30, 50, 75, 100, 125, 150, 250, 500, 750, and 1000 nM). **b** Resolution of fluorescence spectrum versus the CP concentrations; **b** (inset) linear relationship between fluorescence emission and CP (0–30 nM). Selectivity study for CP with coexisting other drugs and compounds' **c** fluorescence spectra and **d** histogram representation and **e** selectivity analysis with other Pt-based drugs **f** study with other most possible coexisting compounds. **g** Visual detection of CP

L-His and MA assay in food sample

We used milk as a typical food sample to test the proposed sensor applicability and reliability. The L-His and MA were spiked into milk samples at three different concentrations. The assay exposed good recovery rates from 97.5.8 to 102.4% and 96.8 to 105%, respectively, which are listed in Table 1. These outcomes indicated that the recovery of the established L-His and MA biosensor was indeed judicious and may have promising applications in the detection of L-His and MA in real food samples.

L-His and CP assay in the biological sample

We used urine as a typical sample to test the proposed sensor's applicability and reliability. Three different concentrations of L-His and CP were spiked into urine samples. The results outlined in Table 2 show that the approach yielded good recovery rates ranging from 98.6 to 105% and 96.4 to 100.4% for the L-His and CP respectively. These findings suggest that the recovery of the well-established L-His and CP biosensor was prudent, and they can find their role in many intriguing applications in the detection of L-His and CP in real biological samples.

Conclusion

In this work, we established a simple and label-free fluorometric sensor for the L-His, MA, and CP detection using DNAzyme-based special label and quencher-free signal amplification technique. Herein, we have also proved that a conventional fluorescent AuO dye can induce and stabilize the G4cpx preferentially across the ssDNA and dsDNA with increased fluorescence signal to detect the L-His and decrease the AuO emission after the addition of MA or CP. The advantage of this approach was that it considerably enhanced the recognition sensitivity, as the LOD could go down to the nanomolar level which was much lower than the EPA limit for the L-His and MA in milk samples and the L-His and CP in the urine samples. Remarkably, this scheme effectively avoided any alteration as well as complex enzymatic or hairpins-based amplification operations. The technique is very selective and facilitates reliable detection of target molecules in the presence of other interference molecules at high concentrations. Consequently, this system demonstrates easy, consistent, and remarkable analytical performance for the specific and sensitive monitoring of the L-His, MA, and CP in actual samples. Thus, we conclude that the proposed sensor probe is deemed to enrich the toolbox for managing L-His, MA, and CP usage. Moreover, this technique provided an adaptable platform for the extremely sensitive detection of other molecules using the respective DNAzymes, as well as a broad range of other non-metal targets by using aptamer and aptazymes.

Table 1 Examination of L-His and MA in the milk samples

Samples	Spiked (nM)	Detected to L-His ± SD	Recovery (%)	Spiked (μM)	Detected to MA ± SD	Recovery (%)
Milk I	2	$2.05^{x} \pm 1.12^{y}$	102.4	0.1	$0.097^{x} \pm 0.02^{y}$	97
	4	$4.06^{x} \pm 0.25^{y}$	101.3	0.2	$0.19^{x} \pm 0.09^{y}$	96.8
	6	$5.97^{x} \pm 1.3^{y}$	99.5	0.3	$0.31^{x} \pm 0.02^{y}$	103.3
Milk II	2	$1.95^{x} \pm 1.12^{y}$	97.5	0.1	$0.10^{x} \pm 0.01^{y}$	100.4
	4	$4.2^{x} \pm 0.25^{y}$	105	0.2	$0.21^{x} \pm 0.03^{y}$	105
	6	$5.99^{x} \pm 1.3^{y}$	99.8	0.3	$0.29^{x} \pm 0.05^{y}$	97.3

x mean values of three determinations, *y* standard deviation

Table 2 Examination of L-His and CP in the urine samples

Samples	Spiked (nM)	Detected to L-His ± SD	Recovery (%)	Spiked (nM)	Detected to CP ± SD	Recovery (%)
Urine I	2	$1.95^{x} \pm 0.12^{y}$	99.4	5	$5.02^{x} \pm 0.22^{y}$	100.4
	4	$4.12^{x} \pm 0.25^{y}$	105.3	10	$9.91^{x} \pm 0.89^{y}$	99.3
	6	$5.99^{x} \pm 1.3^{y}$	99.3	15	$15.05^{x} \pm 0.5^{y}$	100.3
Urine II	2	$2.01^{x} \pm 0.23^{y}$	102.4	5	$4.82^{x} \pm 0.72^{y}$	96.4
	4	$4.16^{x} \pm 0.25^{y}$	101.3	10	$9.60^{x} \pm 1.89^{y}$	97.3
	6	$5.79^{x} \pm 0.53^{y}$	98.6	15	$14.75^{x} \pm 1.5^{y}$	98.3

x mean values of three determinations, *y* standard deviation

Supplementary Information The online version contains supplementary material available at https://doi.org/10.1007/s00216-022-04061-z.

Acknowledgements The authors acknowledge the "Selective Excellence Research Initiative Fund SRMIST-2021" from the Department of Chemistry, SRM Institute of Science and Technology, Tamil Nadu—603 203, India.

Declarations

Conflict of interest The authors declare no competing interests.

References

1. Wu H, Tian D, Fan X, Fan W, Zhang Y, Jiang S, Wen C, Ma Q, Chen N, Xie X. Highly efficient production of L-histidine from glucose by metabolically engineered Escherichia coli. ACS Synth Biol. 2020;9:1813–22.
2. Zheng X, Yao T, Zhu Y, Shi S. Cu^{2+} modulated silver nanoclusters as an on-off-on fluorescence probe for the selective detection of l-histidine. Biosens Bioelectron. 2015;66:103–8.
3. Zhou N, Zhou Q, Meng G, Huang Z, Ke Y, Liu J, Wu N. Incorporation of a basil-seed-based surface enhanced Raman scattering sensor with a pipet for detection of melamine. ACS Sensors. 2016;1:1193–7.
4. Jeong S, Kwon WY, Hwang SH, Shin J, Kim Y, Lee M, Park KS. Fluorescence, turn-on detection of melamine based on its dual functions as fluorescence enhancer of DNA-AgNCs and Hg(II)-scavenger. Artif Cells Nanomed Biotechnol. 2019;47:621–5.
5. Hazra C, Adusumalli VNKB, Mahalingam V. 3,5-Dinitrobenzoic acid-capped upconverting nanocrystals for the selective detection of melamine. ACS Appl Mater Interfaces. 2014;6:7833–9.
6. Mandriota G, Di Corato R, Benedetti M, De Castro F, Fanizzi FP, Rinaldi R. Design and application of cisplatin-loaded magnetic nanoparticle clusters for smart chemotherapy. ACS Appl Mater Interfaces. 2019;11:1864–75.
7. Ma F, Yan S, Zhang J, Wang Y, Wang L, Wang Y, Zhang S, Du X, Zhang P, Chen HY, Huang S. Nanopore sequencing accurately identifies the cisplatin adduct on DNA. ACS Sens. 2021;6:3082–92.
8. Tateda N, Matsuhisa K, Hasebe K, Kitajima N, Miura T. High-performance liquid chromatographic method for rapid and highly sensitive determination of histidine using postcolumn fluorescence detection with o-phthaldialdehyde. J Chromatogr B Biomed Appl. 1998;718:235–41.
9. Venkatasami G, Sowa JR. A Rapid, Acetonitrile-free, HPLC method for determination of melamine in infant formula. Anal Chim Acta. 2010;665:227–30.
10. Lopez-Flores A, Jurado R, Garcia-Lopez P. A high-performance liquid chromatographic assay for determination of cisplatin in plasma, cancer cell, and tumor samples. J Pharmacol Toxicol Methods. 2005;52:366–72.
11. Bhawawet N, Fuangswasdi S, Imyim A. Determination of melamine based on the formation of an insoluble copper-melamine complex and flame atomic absorption spectrometry. Anal Lett. 2014;47:1931–7.
12. Raghavan R, Mulligan JA. Low-level (PPB) determination of cisplatin in cleaning validation (rinse water) samples. I. An Atomic Absorption Spectrophotometric Method. Drug Dev Ind Pharm. 2000;26:423–8.
13. Danielsen M, Nebel C, Dalsgaard TK. Simultaneous determination of L- and D-amino acids in proteins: a sensitive method using hydrolysis in deuterated acid and liquid chromatography–tandem mass spectrometry analysis. Foods. 2020;9:309.
14. Yang SP, Hu B, Li JQ, Han J, Zhang X, Chen HW, Liu Q, Liu QJ, Zheng J. Surface desorption atmospheric pressure chemical ionization mass spectrometry for direct detection melamine in powdered milk products. Fenxi Huaxue/Chin J Anal Chem. 2009;37:691–4.
15. Ming X, Groehler A, Michaelson-Richie ED, Villalta PW, Campbell C, Tretyakova NY. Mass spectrometry based proteomics study of cisplatin-induced DNA-protein cross-linking in human fibrosarcoma (HT1080) cells. Chem Res Toxicol. 2017;30:980–95.
16. Gholivand MB, Ahmadi E, Mavaei M. A novel voltammetric sensor based on graphene quantum dots-thionine/nano-porous glassy carbon electrode for detection of cisplatin as an anti-cancer drug. Sensors Actuators B Chem. 2019;299:126975.
17. Zhang Z, Hu Y, Zhang H, Luo L, Yao S. Layer-by-layer assembly sensitive electrochemical sensor for selectively probing l-histidine based on molecular imprinting sol-gel at functionalized indium tin oxide electrode. Biosens Bioelectron. 2010;26:696–702.
18. Liang X, Wei H, Cui Z, Deng J, Zhang Z, You X, Zhang XE. Colorimetric detection of melamine in complex matrices based on cysteamine-modified gold nanoparticles. Analyst. 2011;136:179–83.
19. Chuaychob S, Thammakhet-Buranachai C, Kanatharana P, Thavarungkul P, Buranachai C, Fujita M, Maeda M. A nanobiosensor for the simple detection of small molecules using noncrosslinking aggregation of gold nanoparticles with G-quadruplexes. Anal Methods. 2020;12:230–8.
20. Pavadai R, Amalraj A, Subramanian S, Perumal P. High catalytic activity of fluorophore-labeled Y-shaped DNAzyme/3D MOF-MoS2NBs as a versatile biosensing platform for the simultaneous detection of Hg^{2+}, Ni^{2+}, and Ag^{+} ions. ACS Appl Mater Interfaces. 2021;13:31710–24.
21. Arunjegan A, Rajaji P, Sivanesan S, Panneerselvam P. A Turn-ON fluorometric biosensor based on SsDNA immobilized with a metal phenolic nanomaterial for the sequential detection of Pb(II) and epirubicin cancer drug. RSC Adv. 2021;11:12361–73.
22. Amalraj A, Pavadai R, Perumal P. Recyclable target metal-enhanced fluorometric naked eye aptasensor for the detection of Pb^{2+} and Ag^{+} ions based on the structural change of $CaSnO_3$ @PDANS-constrained GC-rich SsDNA. ACS Omega. 2021;6:30580–97.
23. Rajaji P, Panneerselvam P. A novel polydopamine grafted 3D MOF nanocubes mediated GR-5/GC DNAzyme complex with enhanced fluorescence emission response toward spontaneous detection of Pb(II) and Ag(I) ions. ACS Omega. 2020;5:25188–98.
24. Amdursky N, Huppert D. Auramine-O as a fluorescence marker for the detection of amyloid fibrils. J Phys Chem B. 2012;116:13389–95.
25. Aydinoglu S, Pasti A, Biver T, Mennucci B. Auramine O interaction with DNA: a combined spectroscopic and TD-DFT analysis. Phys Chem Chem Phys. 2019;21:20606–12.
26. Ravikumar A, Panneerselvam P, Radhakrishnan K. Fluorometric determination of lead (II) and mercury (II) based on their interaction with a complex formed between graphene oxide and a DNAzyme. Microchim Acta. 2017;2:8–15.
27. Xu H, Geng F, Wang Y, Xu M, Lai X, Qu P, Zhang Y, Liu B. A label-free fluorescent molecular switch for a DNA hybridization

assay utilizing a G-quadruplex-selective auramine O. Chem Commun. 2015;51:8622–5.
28. Xie Z, Lei J, Yang M, Li Y, Geng X, Liu S, Wang J. Conical nanofluidic channel for selective quantitation of melamine in combination with β-cyclodextrin and a single-walled carbon nanotube. Biosens Bioelectron. 2019;127:200–6.
29. N'Soukpo-Kossi CN, Descôteaux C, Asselin É, Tajmir-Riahi HA, Bérubé G. DNA interaction with novel antitumor estradiol-platinum(II) hybrid molecule: a comparative study with cisplatin drug. DNA Cell Biol. 2008;27:101–7.
30. Zhang C, Zhang HL, Han MN, Yang XL, Pei CH, Xu ZD, Du J, Li W, Chen S. DNA-affibody nanoparticle delivery system for cisplatin-based breast cancer chemotherapy. RSC Adv. 2019;9:1982–9.

Arunjegan Amalraj is a PhD student at SRM Institute of Science and Technology in Tamil Nadu, India, under the guidance of Dr. Panneerselvam Perumal. He received his Bachelors degree in chemistry from Jaya college of arts and science and Master of science from DG Vaishnav College in Tamil Nadu, India. His research focuses on environmental and food contamination, so he establishes a different biosensor to monitor and control heavy metal and biomolecule contamination in environment and food samples.

Dr. Panneerselvam Perumal is Senior Assistant Professor of the Department of Chemistry, Faculty of Engineering and Technology at SRM Institute of Science and Technology. Tamil Nadu, India. He received his master of science degree in chemistry from the Madurai Kamaraj University, and his PhD in chemistry from Anna University, Tamil Nadu, India. He has worked in Malaysia as a post-doctoral researcher in the School of Industrial Technology and Environmental Technology division. His main research interests are in the development of various nanomaterial-based biosensors, chemosensors, and electrochemical sensors for the detection of heavy metal ions and biomolecules in real-world samples.